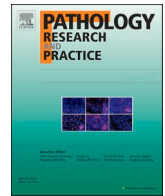


Title	Spatial transcriptome analysis of lung squamous cell carcinoma arising from interstitial pneumonia provides insights into tumor heterogeneity
Author(s)	Ukon, Koto; Nojima, Satoshi; Motooka, Daisuke et al.
Citation	Pathology - Research and Practice. 2025, 266, p. 155805
Version Type	VoR
URL	<a href="https://hdl.handle.net/11094/100394">https://hdl.handle.net/11094/100394</a>
rights	This article is licensed under a Creative Commons Attribution-NonCommercial 4.0 International License.
Note	


*Osaka University Knowledge Archive : OUKA*

<https://ir.library.osaka-u.ac.jp/>

Osaka University



## Spatial transcriptome analysis of lung squamous cell carcinoma arising from interstitial pneumonia provides insights into tumor heterogeneity

Koto Ukon<sup>a,1</sup>, Satoshi Nojima<sup>a,\*,1</sup> , Daisuke Motooka<sup>b,c,d</sup>, Tsuyoshi Takashima<sup>a</sup>, Masaharu Kohara<sup>a</sup>, Hiroki Kiyokawa<sup>a</sup>, Kenji Kimura<sup>e</sup>, Eriko Fukui<sup>e</sup>, Shinichiro Tahara<sup>a</sup>, Kansuke Kido<sup>a</sup>, Takahiro Matsui<sup>a</sup>, Yasushi Shintani<sup>e</sup>, Daisuke Okuzaki<sup>b,c,d</sup>, Eiichi Morii<sup>a,f,\*\*</sup>

<sup>a</sup> Department of Pathology, Osaka University Graduate School of Medicine, Osaka, Japan

<sup>b</sup> Integrated Frontier Research for Medical Science Division, Institute for Open and Transdisciplinary Research Initiatives (OTRI), Osaka University Institute for Open and Transdisciplinary Research Initiatives, Osaka University, Osaka, Japan

<sup>c</sup> Genome Information Research Center, Research Institute for Microbial Diseases, Osaka University, Osaka, Japan

<sup>d</sup> Laboratory of Human Immunology (Single Cell Genomics), WPI Immunology Frontier Research Center, Osaka University, Osaka, Japan

<sup>e</sup> Department of General Thoracic Surgery, Osaka University Graduate School of Medicine, Osaka, Japan

<sup>f</sup> RNA Frontier Science Division, Institute for Open and Transdisciplinary Research Initiatives (OTRI), Osaka University, Osaka, Japan

### ARTICLE INFO

#### Keywords:

Lung squamous cell carcinoma  
Interstitial pneumonia  
Spatial transcriptome  
Glucocorticoid receptor

### ABSTRACT

Interstitial pneumonia (IP) is a refractory disease that causes severe inflammation and fibrosis in the interstitium of the lungs, often resulting in the development of lung cancer (LC) during treatment. Previous studies have demonstrated that the prognosis of LC complicated by IP is inferior to that of LC without IP. It is therefore of the utmost importance to gain a deeper understanding of the heterogeneity of such tumors. In the present study, we conducted spatial transcriptome analysis of squamous cell carcinoma arising from IP. The results suggested involvement of the glucocorticoid receptor pathway in treatment resistance. Immunostaining of squamous cell carcinoma specimens from patients with IP demonstrated that the tumors expressed *NR3C1* to varying degrees. Furthermore, higher *NR3C1* expression levels were associated with a significantly increased risk of recurrence. Our results point to a novel subtype of lung squamous cell carcinoma. Further analysis of the molecular mechanisms associated with this subtype may facilitate the development of novel diagnostic criteria and therapeutic approaches.

### 1. Introduction

Lung cancer (LC) is a significant public health concern, ranking as the second most commonly diagnosed cancer and the leading cause of cancer mortality in 2020 [1]. LC arises from the epithelial cells of the airways. Histological types of LC include adenocarcinoma, squamous cell carcinoma, and small cell carcinoma, which differ in terms of clinical prognosis and sensitivity to anticancer drugs.

Interstitial pneumonia (IP) is a disease in which pathological inflammation and fibrosis occur in the interstitium of the lungs. In addition to IP associated with systemic diseases, such as collagen

diseases, idiopathic IP (i.e., IP with no identifiable cause) is also seen. The rates of progression and response to treatment vary with the type of IP. Idiopathic pulmonary fibrosis, the most frequent form of IP, is refractory and progressive [2,3]. It is well documented in the medical literature that cases of IP are frequently complicated by LC, and the risk of LC is increased in patients with IP [4–7]. Squamous cell carcinoma is the most prevalent histological subtype, followed by adenocarcinoma [7]. The prognosis for patients with LC and IP is less favorable than that for patients with LC alone, even when controlling for cancer stage [8,9]. Subtype affects survival, with patients with LC and IP having worse survival rates than patients with nonspecific IP or cryptogenic

**Abbreviations:** LUSC, Lung squamous cell carcinoma; LC, lung cancer; IP, interstitial pneumonia; NR3C1, nuclear receptor subfamily 3 group C member 1; NSCLC, non-small cell lung cancer; UMAP, uniform manifold approximation and projection; FDR, false discovery rate; FC, fold change.

\* Corresponding author.

\*\* Correspondence to: Department of Pathology, Graduate School of Medicine, Osaka University, 2-2 Yamadaoka, Suita, Osaka 565-0871, Japan.

E-mail addresses: [s.nojima@molpath.med.osaka-u.ac.jp](mailto:s.nojima@molpath.med.osaka-u.ac.jp) (S. Nojima), [morii@molpath.med.osaka-u.ac.jp](mailto:morii@molpath.med.osaka-u.ac.jp) (E. Morii).

<sup>1</sup> Koto Ukon and Satoshi Nojima contributed equally as co-first authors of this article.

<https://doi.org/10.1016/j.prp.2024.155805>

Received 16 October 2024; Received in revised form 20 December 2024; Accepted 29 December 2024

Available online 31 December 2024

0344-0338/© 2024 The Authors. Published by Elsevier GmbH. This is an open access article under the CC BY-NC license (<http://creativecommons.org/licenses/by-nc/4.0/>).

organizing pneumonia [10]. Understanding the heterogeneity of LCs that occur in IP would likely facilitate the treatment and/or diagnosis of these diseases.

Recent developments in spatial transcriptome technology have allowed identification of gene expression profiles in which location information is preserved in various diseases [11,12]. This technology is improving our understanding of the heterogeneity of LCs [13–22]. For example, Kraemer et al. performed deep antigen discovery by combining immunopeptidomic, genomic, bulk, and spatial transcriptomic analyses of tumor regions and adjacent nonmalignant lung tissues from eight patients with LC [13]. The results revealed a higher number of predicted neoantigens within human leukocyte antigen I “hotspots” in clusters of differentiation CD3 + CD8 + T cell-excluded tumors. Zhang et al. conducted spatial RNA sequencing analysis of primary and metastatic non-small cell lung cancer (NSCLC) specimens from 44 patients, which yielded a comprehensive map of the metastatic transcriptome [14]. This map included morphological markers of the tumor core, tumor immune microenvironment, and tumor brain microenvironment. Wang et al. combined spatial transcriptomics and multiplex immunohistochemistry to elucidate the molecular characteristics and cellular plasticity of distinct histological subtypes of lung adenocarcinoma [15]. However, no study has conducted spatial transcriptome analysis of LC arising from IP.

## 2. Materials and methods

### 2.1. Clinical specimens

Lung squamous cell carcinoma (LUSC) tissues were obtained from 37 patients who underwent surgery at Osaka University Hospital between 2017 and 2023. Among them, tissue from one patient was subjected to spatial transcriptome analysis (Visium; 10x Genomics, Pleasanton, CA, USA). The patient, a 78-year-old male, was diagnosed with LUSC subsequent to the development of a nodular lesion while he was undergoing treatment for IP. Indeed, IP with usual interstitial pneumonia (UIP) pattern was observed in the background tumor-free area of the LUSC surgical specimen. Immunostaining was performed on specimens from the 37 patients, including 19 patients with LUSC with IP (LUSC-IP) and 18 patients with LUSC without IP (LUSC-non-IP). In the case of LUSC-IP, 9 cases were classified as recurrent and 10 cases as non-recurrent. Among the 9 cases of recurrent LUSC-IP, tumor recurrence occurred within 1, 2 and 4 years in 6, 2 and 1 cases, respectively. Of the 10 non-recurrent LUSC-IP cases, 4, 4, and 2 cases were confirmed to be recurrence-free for > 3, > 2, and > 1 years, respectively. In the case of LUSC-non-IP, 8 cases were classified as recurrent and 10 cases as non-recurrent. Recurrence occurred within 2 years in all recurrent LUSC non-IP cases. All non-recurrent LUSC-non-IP cases had been free of recurrence for at least 2 years.

### 2.2. Antibodies

Supplementary Table S1 lists the primary antibodies used in this study.

### 2.3. Spatial transcriptome analysis

Spatial transcriptome analysis was performed according to the Visium Spatial Gene Expression Reagent Kits User Guide (CG000239; 10x Genomics). A piece of unfixed LUSC tissue was cut out, and a frozen tissue block was formed using OCT compound. The RNA quality of tissue sectioned from the frozen block was confirmed to meet the requirements for spatial transcriptome analysis (RNA integrity number = 2.50, distribution value 200 > 70 %). After the tissue adhesion test had been performed with the Visium Spatial Imaging Test Slide (PN-2000235), a 10- $\mu$ m-thick tissue section was obtained from the frozen tissue with a microtome and placed onto the capture area (6.5  $\times$  6.5 mm) of the

Visium Spatial Gene Expression Slide (PN-2000233). The tissue section was subjected to hematoxylin and eosin staining, imaging, and decrosslinking, followed by the construction of libraries. The libraries were sequenced on the NovaSeq 6000 System (Illumina, San Diego, CA, USA), running in paired-end mode (read 1: 28 bp, read 2: 90 bp) at a depth of approximately 58,000 reads per spot. Raw FASTQ files and histological images were processed with Space Ranger software (10x Genomics). All subsequent analyses, including graph-based clustering, pathway analysis, and the generation of diagrams of the respective pathways, were conducted using BioTuring Lens – Bulk software (BioTuring, San Diego, CA, USA).

### 2.4. Immunohistochemistry

Sections were cut to a thickness of 4  $\mu$ m and subjected to chromogenic immunohistochemistry using BenchMark GX (Ventana, Tucson, AZ, USA) with an anti-NR3C1 rabbit polyclonal antibody (GTX101120 [1:100 dilution]; GeneTex, Irvine, CA, USA) or an anti-C/EBP Beta (CEBPB) rabbit polyclonal antibody (PB9171 [1:100 dilution]; Boster Bio, Pleasanton, CA, USA) or an anti-C/EBP Delta (CEBPD) rabbit polyclonal antibody (LS-B10190 [1:100 dilution]; LSBio, Newark, CA, USA). The expression levels of the proteins were assessed based on staining intensity under a bright-field microscopy using a visual grading system. No detectable staining, weak staining, and strong staining were scored as 0, 1, and 2, respectively. H-scores were calculated using the following formula: H-score = 0  $\times$  (% cells with a score of 0) + 1  $\times$  (% cells of cells with a score of 1) + 2  $\times$  (% cells with a score of 2). Each H-score was confirmed by three experienced pathologists.

### 2.5. Double staining immunohistochemistry

Sections were cut to a thickness of 4  $\mu$ m and subjected to the double staining Immunohistochemistry. The first staining process was conducted using the DAKO Autostainer Link 48 + (DAKO/Agilent Technologies, Santa Clara, CA, USA) with an anti-NR3C1 rabbit polyclonal antibody (GTX101120 [1:200 dilution]; GeneTex, Irvine, CA, USA). This step used the standard EnVision FLEX DAB+ (DAKO/Agilent Technologies, Santa Clara, CA, USA) as a chromogen. In the second staining, the antigen-antibody reaction was performed by DAKO Autostainer Link 48 + with an anti-CD44 rabbit polyclonal antibody (HPA005785 [1:400 dilution]; Atlas Antibodies, Stockholm, Sweden) or an anti-CD44v9 mouse monoclonal antibody (GTX34523 [1:800 dilution]; GeneTex, Irvine, CA, USA), and the subsequent step was performed manually with DISCOVERY Purple kit (760–229; Ventana, Tucson, AZ, USA) as a chromogen according to the manufacturer’s instructions. Due to the fact that the host animal species for the two antibodies was the same, antibody removal was conducted using the VectaPlex Antibody Removal Kit (VRK-1000; Vector Laboratories, Newark, CA, USA) between the first and second staining in the NR3C1-CD44 double staining process.

### 2.6. Statistical analyses

Most statistical significance was determined using the Mann-Whitney *U* test, performed using EZR software [23]. The only exception is the scoring of the NR3C1-CD44 double staining, where the paired T-test was used since the two populations were normally distributed and showed homoscedasticity. *P*-values < 0.05 were considered significant.

### 2.7. Data availability

The spatial transcriptome data obtained in this study are publicly available in the Gene Expression Omnibus (GEO) (accession number: GSE268015).

### 3. Results

#### 3.1. Spatial transcriptome analysis of LUSC tissue

We first performed gene expression profiling of LUSC tissue using

Visium (10x Genomics) (Fig. 1A). The gene expression profiles of 2104 barcoded spots (55 μm in diameter) under the LUSC tissue were analyzed; 96.0 % of the barcodes and 99.7 % of the unique molecular identifiers were valid (Supplementary Fig. 1, Supplementary Table 2). The barcoded spots were classified into 9 clusters based on their gene

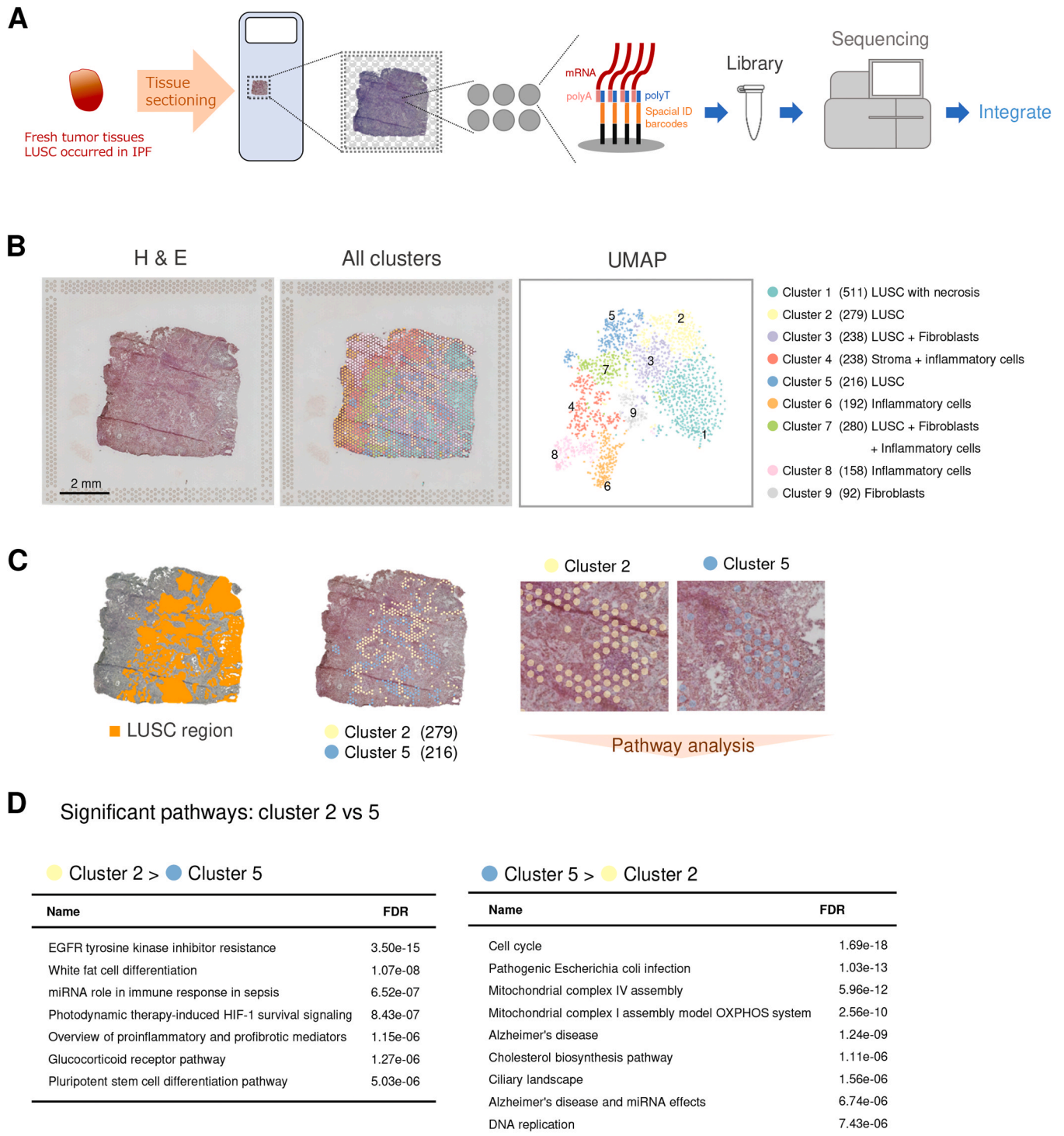


**Fig. 1. Spatial transcriptome analysis of lung squamous cell carcinoma (LUSC) tissue.** (A) Schematic workflow of spatial transcriptome analysis. (B) Results of spatial transcriptome analysis of an LUSC tissue specimen from a patient with interstitial pneumonia. Hematoxylin and eosin staining (left), gene expression profiles of 2104 barcoded spots (middle), and Uniform Manifold Approximation and Projection (UMAP) visualization (right) are presented. Whole tissues were classified via graph-based clustering. (C) Histological image of cancerous areas, colored orange (left), and an image representing the two clusters identified as representative of LUSC (right). (D) The top seven upregulated pathways in cluster 2 compared to cluster 5 (left), and the top nine pathways upregulated in cluster 5 compared to cluster 2 (right). Only pathways where the false discovery rate (FDR) was < 1.0e-5 are presented.



expression patterns (Fig. 1B). Hematoxylin and eosin images indicated that clusters 2 and 5 were mostly composed of LUSC cells (Fig. 1C). Cluster 1 consisted of LUSC tissue with severe necrosis. Cluster 3 contained fibroblastic tissue at the border in addition to the tumor. Cluster 7 included LUSC, fibroblasts, and inflammatory cells. Cluster 4 consisted mainly of stromal tissue with inflammatory cell infiltration. Clusters 6 and 8 were dominated by clusters of inflammatory cells. Cluster 9 mostly comprised fibrotic tissue. Pathway analysis was conducted for genes with significant expression differences between clusters 2 and 5, and multiple pathways of interest were identified (Fig. 1D). Pathways with stronger relationships with cluster 2 than with cluster 5 included “EGFR tyrosine kinase inhibitor resistance,” “photodynamic therapy-induced HIF-1 survival signaling,” and “pluripotent stem cell differentiation.” Therefore, cluster 2 was considered to be closely associated with the highly treatment-resistant LUSC subtype. The “EGFR tyrosine kinase inhibitor resistance” pathway was characterized by high expression levels of genes including *RPS6*, *VEGFA*, *EIF4EBP1*, and *FGFR3* (Supplementary Table 3). The “photodynamic therapy-induced HIF-1 survival signaling” pathway was characterized by high expression of genes including *IGFBP2*, *SLC2A1*, *IGFBP3*, and *LDHA*, and the “pluripotent stem cell differentiation” pathway was characterized by high expression of genes including *VEGFA*, *INHBA*, *FST*, and *WNT7B*. Pathways associated with cancer cell proliferation and metabolism, including “cell cycle,” “DNA replication,” and “cholesterol biosynthesis,” were more closely associated with cluster 5 than cluster 2 (Fig. 1D). The “cell cycle” pathway was characterized by high expression

levels of genes including *SFN*, *YWHAZ*, *CDKN2A*, and *RBX1* (Supplementary Table 4), the “DNA replication” pathway by high expression of genes including *UBA52*, *UBC*, *RPA3*, and *MCM7*, and the “cholesterol biosynthesis” pathway by high expression of genes including *HMGCS1*, *FDPS*, *SQLE*, and *CYP51A1*. These results suggest that cluster 5 represents the actively proliferating LUSC subtype. The “mitochondrial complex IV assembly” and “mitochondrial complex I assembly model OXPHOS system” pathways were also identified, possibly due to the increased apoptosis of LUSC cells within cluster 5 (in association with their high growth rate); genes related to mitochondria often exhibit high expression levels in spatial transcriptome analyses when cells are undergoing apoptosis [https://kb.10xgenomics.com/hc/en-us/articles/360001086611-Why-do-I-see-a-high-level-of-mitochondrial-gene-expression]. The “Alzheimer’s disease” and “Alzheimer’s disease and miRNA effects” pathways were screened based on their high expression levels of genes encoding tubulin, such as *TUBB*, *TUBA1B*, and *TUBA1C*, as well as *GAPDH* and *CALM1*.

Analysis of the gene expression patterns in clusters 2 and 5 provided additional insights into the heterogeneity of LUSC. The *MKI67* gene, which encodes the well-known proliferation marker Ki-67, was significantly upregulated in cluster 5 compared to cluster 2 (Fig. 2A). The expression level of the *VIM* gene, which encodes vimentin, was significantly higher in cluster 2 than in cluster 5. Conversely, the expression level of *CDH1*, which encodes E-cadherin, was lower in cluster 2 than in cluster 5 (Fig. 2B). These results suggest that the epithelial-mesenchymal transition was more strongly induced in cluster

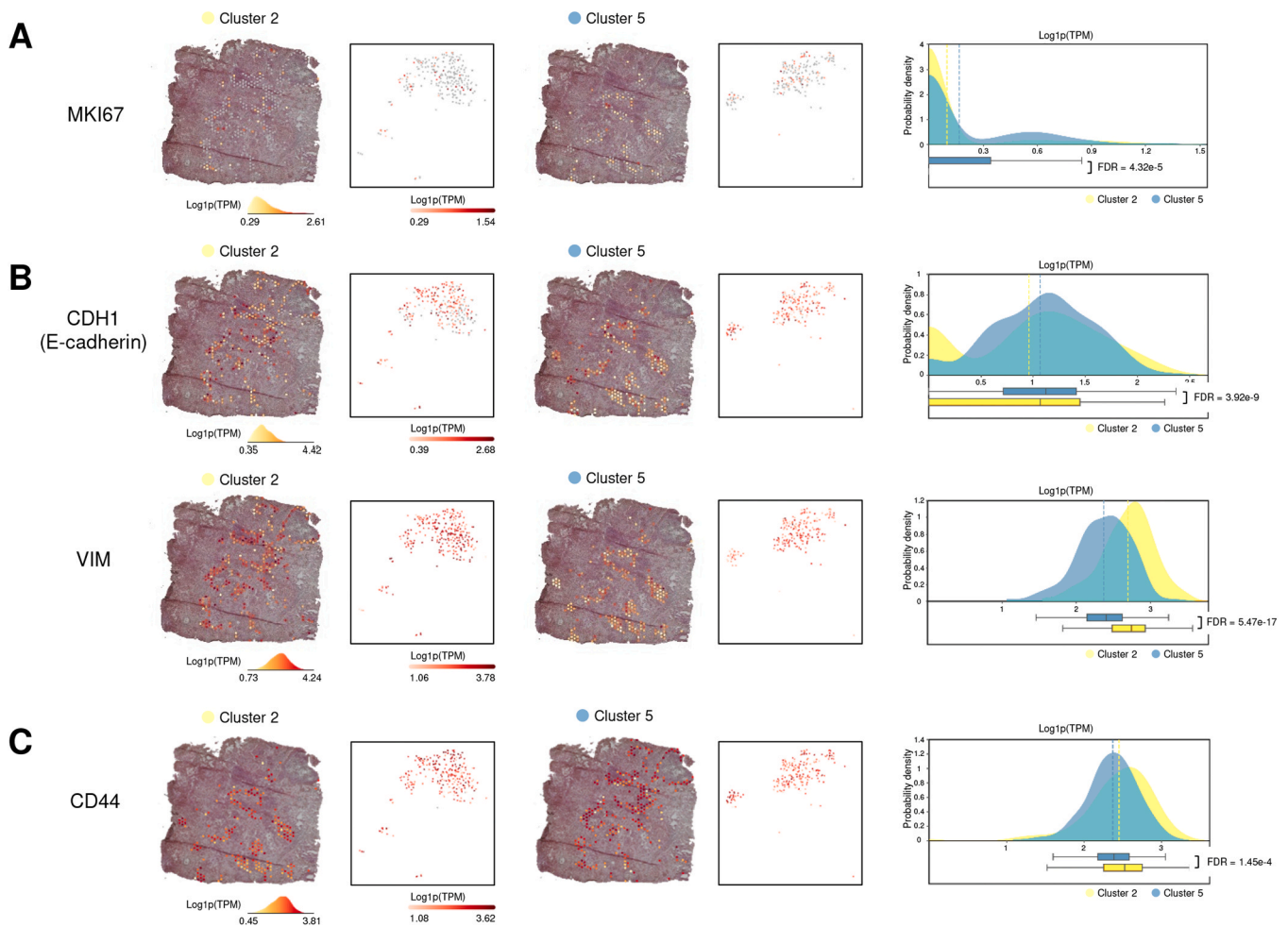


**Fig. 2.** Expression levels of key phenotypic genes in clusters representing LUSC. The expression levels of *MKI67* (A), *CDH1*, *VIM* (B), and *CD44* (C) were evaluated in clusters 2 and 5. A gene expression heatmap (Log<sub>1p</sub>(TPM)) is presented for barcoded spots from clusters 2 and 5 in the histological images and UMAP visualization. Histograms of gene expression levels are also presented, along with Log<sub>2</sub> fold change [FC] and FDR values.

2 than in cluster 5. Moreover, *CD44*, the transcript of which has been identified as a cell surface marker for cancer stem cells, was significantly upregulated in cluster 2 compared to cluster 5 (Fig. 2C).

### 3.2. Differential expression of genes in the “glucocorticoid receptor” pathway

Among the pathways identified as differential between clusters 2 and 5, we focused on the “glucocorticoid receptor” pathway because its

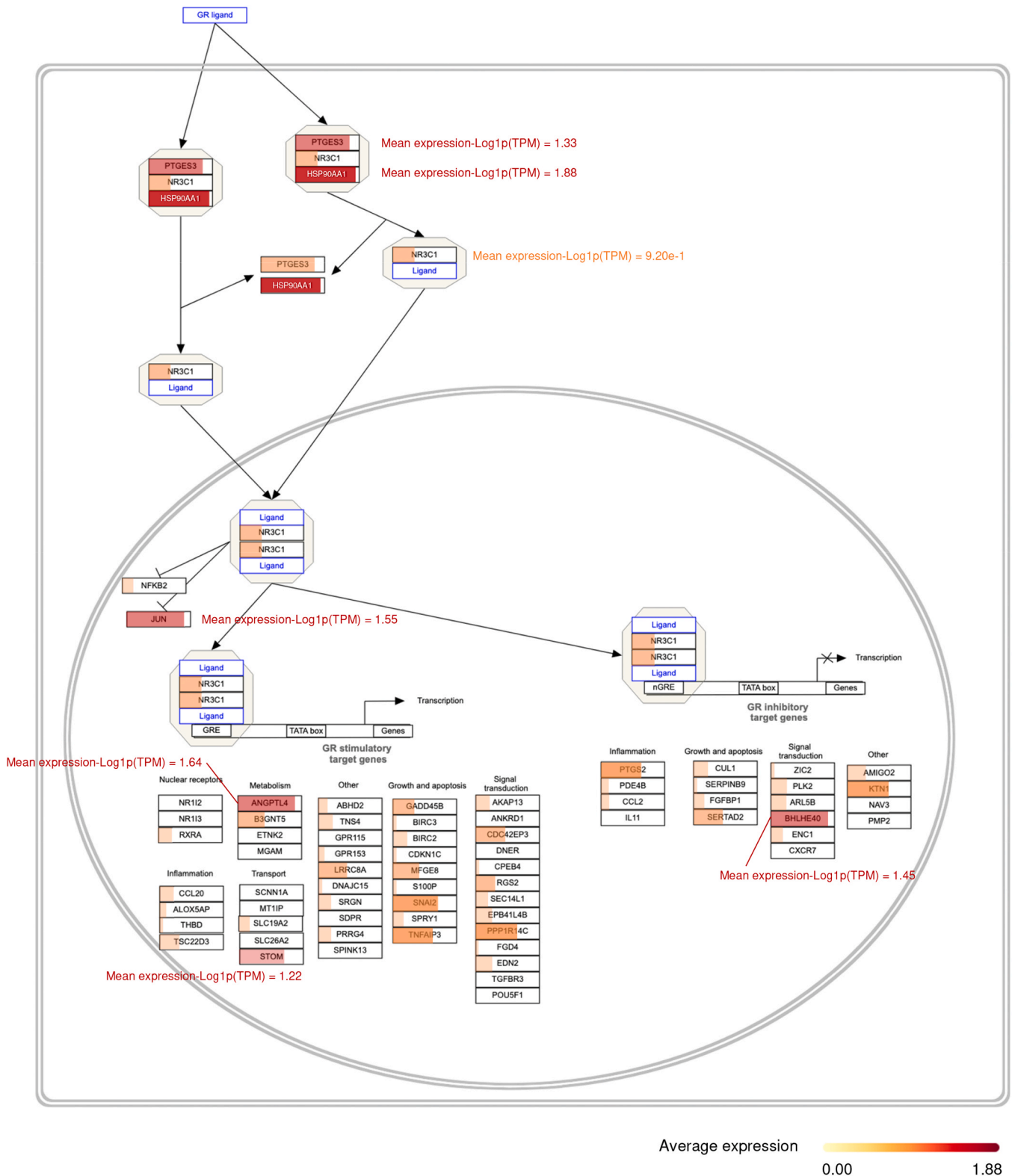


**Fig. 3. Diagram of the glucocorticoid receptor pathway.** The genes in the glucocorticoid receptor pathway, together with their enrichment scores, are presented in diagrams taken from the WikiPathways database. The mean log1p(TPM) values are displayed for genes exhibiting particularly high scores in cluster 2.

significance for tumor heterogeneity was difficult to determine. Following an in-depth analysis of the expression changes of the individual genes included in the "glucocorticoid receptor" pathway, we discovered that *NR3C1*, which encodes the glucocorticoid receptor, demonstrated an increased expression in cluster 2 in comparison to cluster 5 (false discovery rate [FDR] =  $5.76 \times 10^{-7}$ ) (Fig. 3, Fig. 4). Other genes, including *PTGES3*, *HSP90AA1*, *JUN*, *ANGPTL4*, *STOM*, and *BHLHE40*, were also upregulated in cluster 2 (Fig. 3).

### 3.3. Immunohistochemical analysis of *NR3C1* in human LUSC tissue

Furthermore, we performed immunostaining of additional patient-derived LUSC tissue to determine the protein-level expression of *NR3C1* (Fig. 5, Table 1). The expression of *NR3C1* in LUSC varied considerably between cases. Even in a specimen derived from a single patient, some components exhibited strong staining, whereas others exhibited weak or no staining (Fig. 5A). We then evaluated the expression levels of *NR3C1* in tissues of LUSC with or without IP according to the H-scores (percentage of positive tumor cells  $\times$  staining intensity value) (Fig. 5B). In LUSC with IP (LUSC-IP) cases, the H-score was significantly higher for LUSC cases with recurrence versus those without (Fig. 5C,D). The H-score of recurrent cases of LUSC-IP was significantly higher than that of cases of LUSC without IP (LUSC-non-IP), with or without recurrence. Next, we estimated the potential risk of recurrence and overall survival of LUSC-IP patients using the Kaplan–Meier method. High immunohistochemical expression levels of *NR3C1* were associated with a higher risk of recurrence ( $p = 0.0196$ ; Fig. 5E), and we observed a trend toward a negative association between *NR3C1* expression and overall survival ( $p = 0.0745$ ; Fig. 5F). These results support the notion that the tumor subtype characterized by high *NR3C1* expression contributes to the heterogeneity in high-grade malignancy seen among patients with LUSC and IP.

In light of the spatial transcriptome analysis results, which indicated elevated CD44 expression in Cluster 2 (Fig. 2C), we conducted an

evaluation of the co-expression of *NR3C1* and CD44 using the specimens of LUSC-IP cases. We performed double immunostaining of *NR3C1* and CD44 or one of its isoform variants, CD44v9, which is known to be particularly highly expressed in cancer stem cells (Fig. 5G,H). The expression levels of CD44 and CD44v9 were evaluated between LUSC components that express high levels of *NR3C1* and those that do not express *NR3C1*. The results demonstrated that both CD44 and CD44v9 were highly expressed in the tumor components that express high levels of *NR3C1*.

We also focused on another intriguing pathway, the "white fat cell differentiation" pathway, which is centered on two transcription factors: *CEBPB* and *CEBPD*. The expression levels of the genes encoding these factors were found to be elevated in cluster 2 (Supplementary Fig. 2). However, when the expression levels of these molecules were compared between LUSC cases with and without recurrence, no statistically significant differences were found (Supplementary Fig. 3).

### 3.4. Analysis for the tumor microenvironment with spatial transcriptome data

Finally, we once more employed spatial transcriptome data to obtain insights into the tumor microenvironment. The expression levels of tumor-associated macrophages (TAMs) were evaluated in clusters 3, 4, and 7, which are in close proximity to the tumor clusters, namely clusters 2 and 5 (Fig. 6A). The analysis revealed that both macrophage markers and markers of M2 macrophages, which are regarded as the predominant phenotype of TAM, exhibited high expression levels in cluster 4 (Fig. 6B,C). The morphological evaluation indicated that cluster 4 contained a large amount of vascular endothelium. The high expression of endothelial markers in cluster 4, as observed in the spatial transcriptome data, provided further evidence to support this hypothesis (Fig. 6D). The findings suggest that there is a correlation between TAM-rich areas and the microenvironment with active vascular endothelial neogenesis.

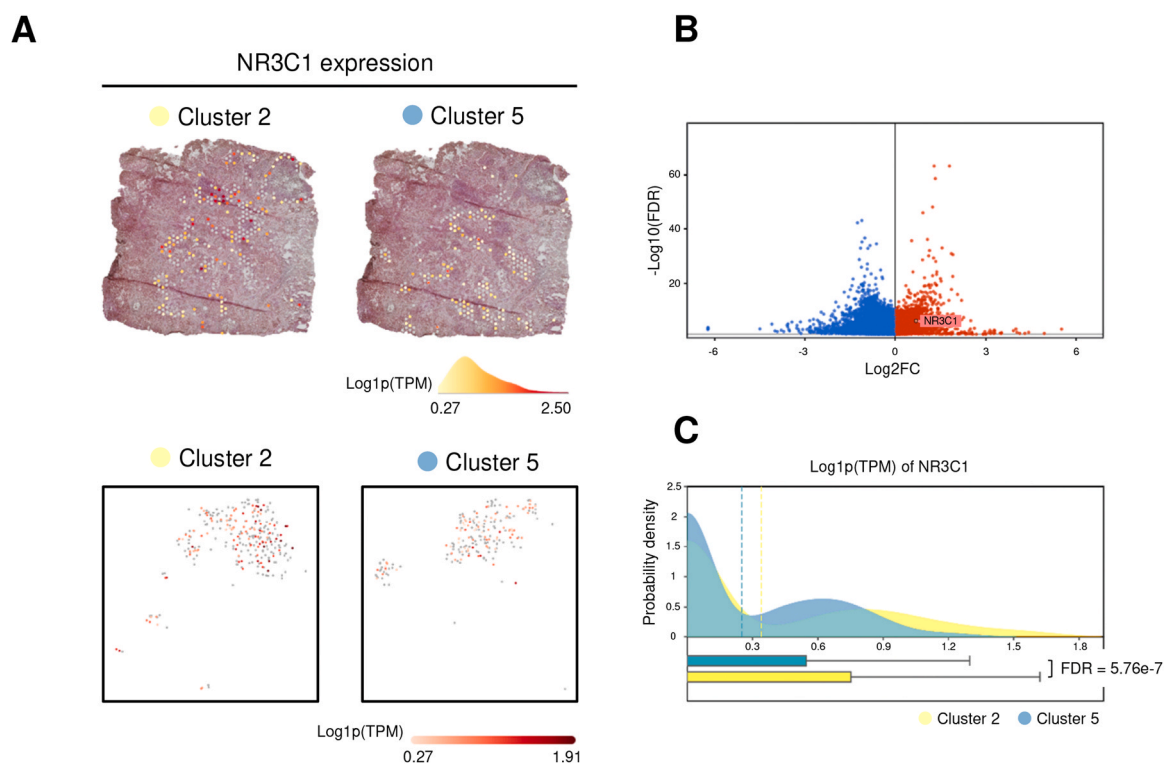


**Fig. 4. Expression of *NR3C1* in clusters representing LUSC.** (A) Expression level of *NR3C1* was evaluated in clusters 2 and 5. A gene expression heatmap (Log<sub>10</sub> [TPM]) is presented for barcoded spots from clusters 2 and 5 in the histological images and UMAP visualization. (B) Volcano plot of *NR3C1* expression. (C) Histograms of gene expression levels, including Log<sub>2</sub> FC and FDR values.



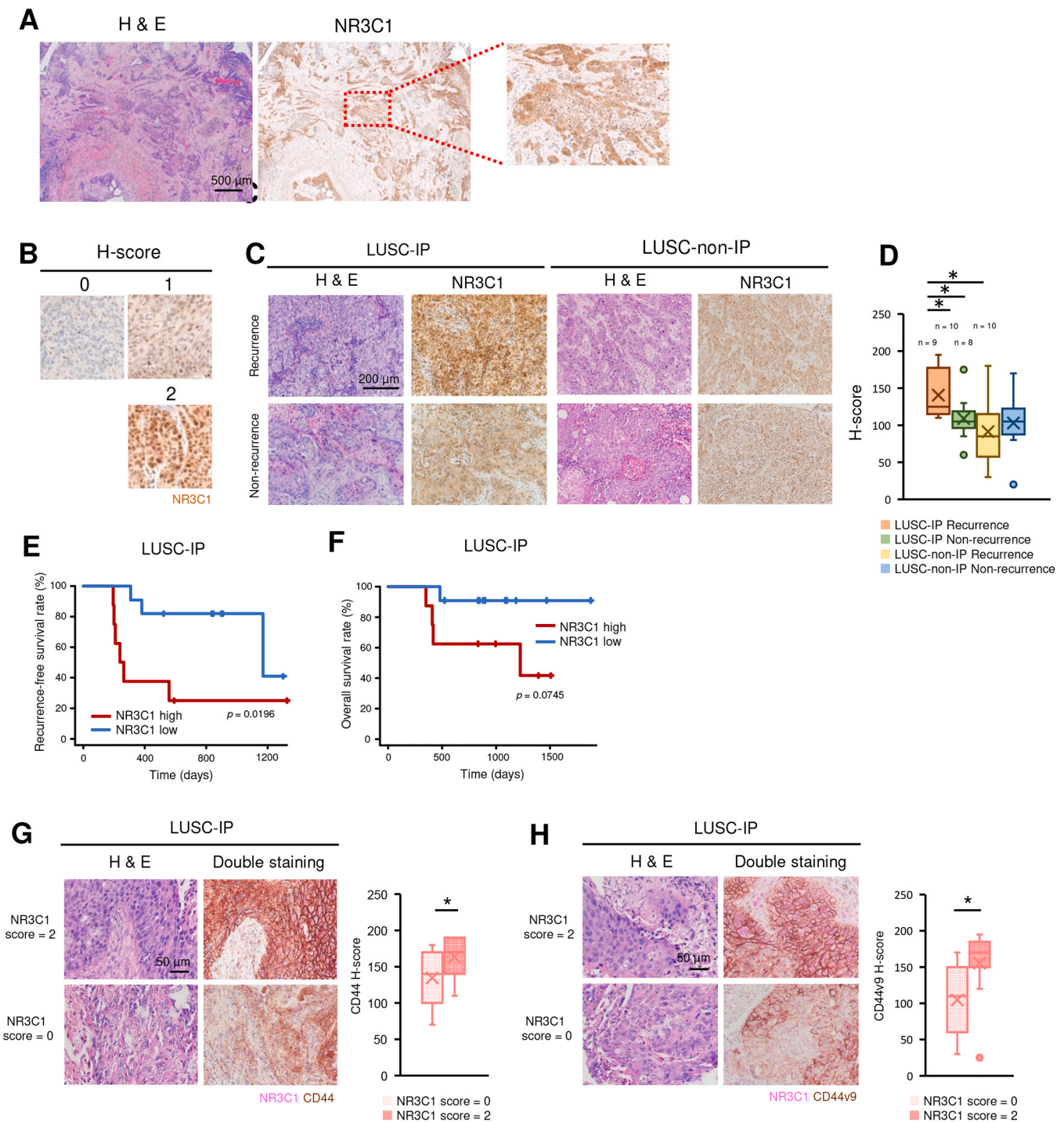


**Fig. 5. NR3C1 expression in LUSC tissue.** (A) Representative hematoxylin and eosin (H & E) and immunohistochemistry images showing NR3C1 expression. Scale bar, 500  $\mu$ m. (B) Representative immunohistochemistry images of NR3C1 expression according to H-scores [H-score = 0  $\times$  (% cells with a score of 0) + 1  $\times$  (% cells of cells with a score of 1) + 2  $\times$  (% cells with a score of 2)]. Following confirmation of the presence of signals in both the nucleus and cytoplasm, the H-scores were calculated by combining these findings. (C) Representative images of LUSC with IP (LUSC-IP) or LUSC without IP (LUSC-non-IP) histology from cases with and without recurrence. Scale bar, 200  $\mu$ m. (D) Boxplot of NR3C1 H-scores calculated for recurrent and non-recurrent LUSC-IP and LUSC-non-IP cases. Center lines indicate medians, box limits indicate the 25th and 75th percentiles, and crosses indicate means. The Mann-Whitney *U* test was used for statistical analyses. \**p* < 0.05. (E) Kaplan-Meier plot of recurrence-free survival. The log-rank test was performed for further analysis. (F) Kaplan-Meier plot of overall survival. The log-rank test was performed for further analysis. (G) Representative H & E and double staining immunohistochemistry images demonstrating NR3C1 and CD44 co-expression and a boxplot illustrating the statistical analysis. This analysis utilized specimens from 11 LUSC-IP cases with both a component exhibiting high NR3C1 expression (equivalent to H-score =2) and a component with no expression (equivalent to H-score =0) among the cases utilized in Fig. 5C. The specimens were then subjected to NR3C1-CD44 double staining immunohistochemistry. LUSC components with high expression of NR3C1 and those without expression were divided into regions, and the signal intensity of CD44 expression in each component was scored and statistically compared in the same manner as in Fig. 5D. Scale bar, 50  $\mu$ m. The Paired T-test was used for statistical analyses. \**p* < 0.05. (H) The same analysis was done for NR3C1-CD44v9 (CD44 variant isoform 9) double staining. Scale bar, 50  $\mu$ m. The Mann-Whitney *U* test was used for statistical analyses. \**p* < 0.05.



**Table 1**  
Clinicopathological characteristics of LUSC patients.

Characteristic	LUSC with IP cases (LUSC-IP)		p-value	LUSC without IP cases (LUSC-non-IP)		p-value
	Recurrence	Non-recurrence		Recurrence	Non-recurrence	
Total, n	9	10		8	10	
Age at operation (y)	72.89 ± 7.78	71.5 ± 7.40	0.71	73.5 ± 6.06	70.2 ± 7.25	0.48
Male	6	10		8	9	
Female	3	0		0	1	
T classification			0.12			0.06
pT1	3	6		1	4	
pT2	3	4		3	5	
pT3	2	0		2	1	
pT4	1	0		2	0	
N classification			0.25			0.45
pN0	5	8		6	9	
pN1	3	2		2	1	
pN2	1	0		0	0	
M classification			N/C			N/C
cM0	8	8		8	10	
cM1	0	0		0	0	
cMX	1	2		0	0	

Clinicopathological characteristics of the patients included in the analysis. p-values were determined by Mann-Whitney U test. N/C, Not calculable.

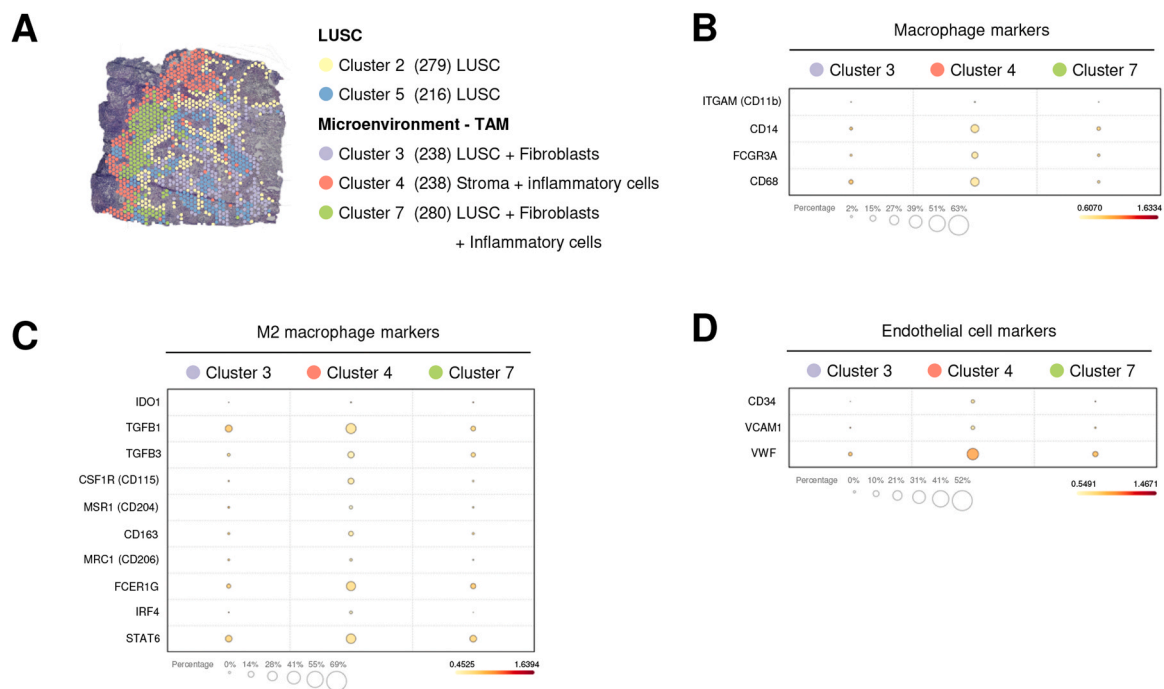


**Fig. 6.** Analysis of tumor-associated macrophages with spatial transcriptome data. (A) Clusters of LUSC (clusters 2, 5) and clusters histologically including inflammatory cells in the tumor microenvironment (clusters 3, 4, 7) in the transcriptome data. (B) Bubble heatmap showing the expression levels of the macrophage marker genes in clusters 3, 4, and 7. (C) Bubble heatmap showing the expression levels of the M2 macrophage marker genes in clusters 3, 4, and 7. (D) Bubble heatmap showing the expression levels of the vascular endothelial cell marker genes in clusters 3, 4, and 7.

Further analysis was conducted on clusters 3 and 9, which exhibited morphological characteristics indicative of fibroblast presence (Supplementary Fig. 4 A). Cluster 9 showed increased expression of cancer-associated fibroblast (CAF) markers, including ACTA2 ( $\alpha$ SMA) and PDGFRB, in comparison to Cluster 3 (Supplementary Fig. 4B). However, the morphological evaluation indicated that cluster 3 consisted of both LUSC cells and fibroblasts. Therefore, the observed difference in CAF marker expression levels between cluster 3 and cluster 9 may be attributed to the varying proportion of fibroblasts. Our analysis did not yield any new insights beyond those already presented.

#### 4. Discussion

In this study, we performed spatial transcriptome analysis of LUSC tissue from a patient with IP in whom LUSC developed during follow-up. Two clusters were identified as representative of LUSC (Fig. 1B,C). One of these clusters was considered to be a treatment-resistant subtype. Comparison of the two clusters via pathway analysis suggested the involvement of several pathways (Fig. 1D). More detailed pathological analyses focusing on one of these pathways, the "glucocorticoid receptor" pathway, revealed that increased expression of *NR3C1* in LUSC was associated with a higher risk of recurrence (Fig. 5).

A number of studies conducted by other research groups have demonstrated the clinicopathological significance of the upregulated

expression of *NR3C1* in LC. For example, Caratti et al. reported that *NR3C1* associates with RAS complexes to inhibit cell proliferation and tumor growth in NSCLC [24]. Dorso et al. found that *NR3C1* and *FOXA1* cooperate to regulate genes involved in epidermal growth factor signaling and G1-S cell cycle progression in NSCLC [25]. Kay et al. reported that loss of *NR3C1* expression due to DNA methylation prevents apoptosis in human small cell LC cells [26]. However, the present study is the first to focus on *NR3C1* expression in LUSC arising from IP.

Our pathway analysis also revealed candidate genes/molecules potentially involved in *NR3C1* signaling (Fig. 3). The expression levels of genes such as *PTGES3*, *HSP90AA1*, *JUN*, and *ANGPTL4* were significantly increased in LUSC tissue. *PTGES3* encodes prostaglandin E synthase 3, which is known to play a role in the proper functioning of glucocorticoid receptors and other steroid receptors [27]. Some studies have reported that high expression of *PTGES3* is associated with poor prognosis and immune cell infiltration in lung adenocarcinoma [28,29]. *HSP90AA1* encodes heat shock protein 90- $\alpha$ , which functions as a chaperone for *NR3C1* [30]. Niu et al. reported that high expression of *HSP90AA1* in cancer tissues was correlated with poorer overall survival and inhibition of HSP90-induced apoptosis through the AKT1/ERK pathway in LC [31]. Notably, differentially expressed genes in patients with LUSC, with or without chronic obstructive pulmonary disease, were investigated on the basis of microarray gene expression profiles in bronchial epithelium, and *HSP90AA1* was identified as a significant gene in the GEO repository [32]. Jun is a transcription factor protein encoded by the *JUN* gene that is widely recognized as a critical molecule in carcinogenesis. A study of NSCLC revealed that Jun was overexpressed in 31 % of cases of primary and metastatic lung tumors [33]. Several studies have shown that angiotensin-like 4, encoded by *ANGPTL4*, is involved in the metastasis, lymphatic/venous invasion, and anoikis resistance of esophageal, head and neck, and oral squamous cell carcinomas [34–40]. The *NR3C1* signaling seen in cases of LUSC with IP may also involve these molecular mechanisms.

Our pathway analysis also suggested the involvement of another signaling pathway, “white adipocyte differentiation,” in the tumor subtype characterized by treatment resistance. This pathway is centered on two transcription factors: *CEBPB* and *CEBPD* (Fig. 1D, Supplementary Fig. 2). Despite our immunohistological analysis indicating that both *CEBPB* and *CEBPD* are frequently expressed in LUSC arising from IP, no significant association was observed between their expression levels and the risk of recurrence (Supplementary Fig. 3). However, these results do not necessarily rule out the importance of *CEBPB*- and *CEBPD*-dependent signaling in LUSC heterogeneity. More detailed functional molecular biology analysis of a larger number of clinical samples will be required before definitive conclusions can be drawn.

This study had some limitations. First, because our spatial transcriptome analysis was based on a single case, it is questionable whether the results are generalizable. Additional spatial transcriptome studies including more cases are needed to validate our findings. Second, the spatial transcriptome data revealed that some clusters, particularly those within the tumor microenvironment, comprised a multitude of cell types. This complexity posed a challenge in conducting a comprehensive assessment of gene expression changes across each subpopulation. Indeed, while we did gain some insight into TAM (Fig. 6), we were unable to identify any new findings on CAF (Supplementary Fig. 4). Precise analysis of such clusters would be possible if the resolution of spatial transcriptome techniques was improved.

## 5. Conclusion

In conclusion, our spatial transcriptome analysis of a LUSC tissue specimen from a patient with IP identified a novel tumor subtype associated with *NR3C1* signaling. Clarification of the molecular mechanisms underlying this phenotype could lead to the establishment of new diagnostic criteria and treatments.

## Ethics approval and consent to participate

Informed consent was obtained from all patients. All of our experimental protocols involving human specimens were approved by the Ethics Review Board of the Graduate School of Medicine, Osaka University (approval no. 15234) and carried out in accordance with the committee’s guidelines and regulations. The study was performed in accordance with the Declaration of Helsinki.

## Funding

This work was supported by JSPS KAKENHI (grant numbers A23H027000, T22K194330, and T21K069030), AMED (JP21ae0121049), and Takeda Science Foundation (2024046036).

## CRediT authorship contribution statement

**Eiichi Morii:** Writing – review & editing, Validation, Supervision, Project administration, Funding acquisition, Conceptualization. **Koto Ukon:** Resources, Investigation, Formal analysis, Data curation. **Daisuke Okuzaki:** Writing – review & editing, Methodology, Data curation. **Satoshi Nojima:** Writing – original draft, Investigation, Funding acquisition, Formal analysis, Data curation, Conceptualization. **Yasushi Shintani:** Supervision, Resources. **Takahiro Matsui:** Validation, Resources. **Kenji Kimura:** Resources. **Masaharu Kohara:** Investigation. **Hiroki Kiyokawa:** Validation, Investigation. **Tsuyoshi Takashima:** Validation, Resources. **Daisuke Motooka:** Writing – review & editing, Methodology, Data curation. **Kansuke Kido:** Validation, Data curation. **Shinichiro Tahara:** Validation, Data curation. **Eriko Fukui:** Resources.

## Declaration of Competing Interest

The authors declare that they have no known competing financial interests or personal relationships that could have appeared to influence the work reported in this paper.

## Acknowledgments

We thank Ms. Takako Sawamura, and Ms. Megumi Nihei from the Department of Pathology, Osaka University Graduate School of Medicine for their technical assistance. This study was supported by Mr. Eiji Oiki, Center for Medical Research and Education, Graduate School of Medicine, Osaka University.

## Registry and the registration No. of the study/trial

Not applicable.

## Animal studies

Not applicable.

## Appendix A. Supporting information

Supplementary data associated with this article can be found in the online version at [doi:10.1016/j.prp.2024.155805](https://doi.org/10.1016/j.prp.2024.155805).

## Data availability

The spatial transcriptome data obtained in this study are publicly available in the Gene Expression Omnibus (GEO) (accession number: GSE268015).

## References

- [1] H. Sung, J. Ferlay, R.L. Siegel, M. Laversanne, I. Soerjomataram, A. Jemal, F. Bray, Global cancer statistics 2020: GLOBOCAN estimates of incidence and mortality worldwide for 36 cancers in 185 countries, *CA: Cancer J. Clin.* 71 (2021) 209–249.
- [2] B. Ley, H.R. Collard, Epidemiology of idiopathic pulmonary fibrosis, *Clin. Epidemiol.* 5 (2013) 483–492.
- [3] T. Araki, H. Katsura, M. Sawabe, K.A. Kida, Clinical study of idiopathic pulmonary fibrosis based on autopsy studies in elderly patients, *Intern Med (Tokyo, Jpn.)* 42 (2003) 483–489.
- [4] W.I. Choi, S.H. Park, B.J. Park, C.W. Lee, Interstitial lung disease and lung cancer development: a 5-year nationwide population-based study, *Cancer Res Treat.* 50 (2018) 374–381.
- [5] R. Hubbard, A. Venn, S. Lewis, J. Britton, Lung cancer and cryptogenic fibrosing alveolitis. A population-based cohort study, *Am. J. Respir. Crit. Care Med* 161 (2000) 5–8.
- [6] H. Matsushita, S. Tanaka, Y. Saiki, M. Hara, K. Nakata, S. Tanimura, J. Banba, Lung cancer associated with usual interstitial pneumonia, *Pathol. Int* 45 (1995) 925–932.
- [7] A. Jafarinezhad, M.H. Yektakooshali, Lung cancer in idiopathic pulmonary fibrosis: a systematic review and meta-analysis, *PLoS One* 13 (2018) e0202360.
- [8] H. Alomaish, Y. Ung, S. Wang, P.N. Tyrrell, S.A. Zahra, A. Oikonomou, Survival analysis in lung cancer patients with interstitial lung disease, *PLoS One* 16 (2021) e0255375.
- [9] T. Lee, J.Y. Park, H.Y. Lee, Y.J. Cho, H.I. Yoon, J.H. Lee, S. Jheon, C.T. Lee, J. S. Park, Lung cancer in patients with idiopathic pulmonary fibrosis: clinical characteristics and impact on survival, *Respir. Med* 108 (2014) 1549–1555.
- [10] M. Kreuter, S. Ehlers-Tenenbaum, M. Schaaf, U. Oltmanns, K. Palmowski, H. Hoffmann, P.A. Schnabel, C.P. Heußel, M. Puderbach, F.J. Herth, A. Warth, Treatment and outcome of lung cancer in idiopathic interstitial pneumonias, *Sarcoidosis Vasc. Diffus. Lung Dis.* 31 (2015) 266–274.
- [11] P.L. Ståhl, F. Salmén, S. Vickovic, A. Lundmark, J.F. Navarro, J. Magnusson, S. Giacomello, M. Asp, J.O. Westholm, M. Huss, A. Mollbrink, S. Linnarsson, S. Codeluppi, A. Borg, F. Pontén, P.I. Costea, P. Sahlén, J. Mulder, O. Bergmann, J. Lundberg, J. Frisén, Visualization and analysis of gene expression in tissue sections by spatial transcriptomics, *Science* 353 (2016) 78–82.
- [12] L. Larsson, J. Frisén, J. Lundberg, Spatially resolved transcriptomics adds a new dimension to genomics, *Nat. Methods* 18 (2021) 15–18.
- [13] A.I. Kraemer, C. Chong, F. Huber, H. Pak, B.J. Stevenson, M. Müller, J. Michaux, E. R. Altamiras, S. Rusakiewicz, L. Simó-Riudalbas, E. Planet, M. Wiznerowicz, J. Dagher, D. Trono, G. Coukos, S. Tissot, M. Bassani-Sternberg, The immunopeptidome landscape associated with T cell infiltration, inflammation and immune editing in lung cancer, *Nat. Cancer* 4 (2023) 608–628.
- [14] Q. Zhang, R. Abdo, C. Iosef, T. Kaneko, M. Cecchini, V.K. Han, S.S. Li, The spatial transcriptomic landscape of non-small cell lung cancer brain metastasis, *Nat. Commun.* 13 (2022) 5983.
- [15] Y. Wang, B. Liu, Q. Min, X. Yang, S. Yan, Y. Ma, S. Li, J. Fan, Y. Wang, B. Dong, H. Teng, D. Lin, Q. Zhan, N. Wu, Spatial transcriptomics delineates molecular features and cellular plasticity in lung adenocarcinoma progression, *Cell Discov.* 9 (2023) 96.
- [16] M. Peressini, R. García-Campelo, B. Massuti, C. Martí, M. Cobo, V. Gutiérrez, M. Dómine, J. Fuentes, M. Majem, J. de Castro, J.F. Córdoba, M.P. Diz, D. Isla, E. Esteban, E. Carcereny, L. Vila, A. Moreno-Vega, S. Ros, A. Moreno, F.J. García, G. Huidobro, C. Aguado, V. Cebery-López, J. Valdivia, R. Palmero, P. Lianes, M. López-Brea, O.J. Vidal, M. Provencio, E. Arriola, J. Baena, M. Herrera, H. Bote, M. Molero, V. Adradas, S. Ponce-Aix, A. Nuñez-Buiza, Á. Uvero, S. Hernandez, F. Lopez-Rios, E. Conde, L. Paz-Ares, J. Zugazagoitia, Spatially preserved multi-region transcriptomic subtyping and biomarkers of chemioimmunotherapy outcome in extensive-stage small cell lung cancer, *Clin. Cancer Res* 30 (2024) 3036–3049.
- [17] L. Xie, H. Kong, J. Yu, M. Sun, S. Lu, Y. Zhang, J. Hu, F. Du, Q. Lian, H. Xin, J. Zhou, X. Wang, C.A. Powell, F.R. Hirsch, C. Bai, Y. Song, J. Yin, D. Yang, Spatial transcriptomics reveals heterogeneity of histological subtypes between lepidic and acinar lung adenocarcinoma, *Clin. Transl. Med* 14 (2024) e1573.
- [18] C. Chen, Q. Guo, Y. Liu, Q. Hou, M. Liao, Y. Guo, Y. Zang, F. Wang, H. Liu, X. Luan, Y. Liang, Z. Guan, Y. Li, H. Liu, X. Dong, X. Zhang, J. Liu, Q. Xu, Single-cell and spatial transcriptomics reveal POSTN(+) cancer-associated fibroblasts correlated with immune suppression and tumour progression in non-small cell lung cancer, *Clin. Transl. Med* 13 (2023) e1515.
- [19] Y. Haga, Y. Sakamoto, K. Kajiya, H. Kawai, M. Oka, N. Motoi, M. Shirasawa, M. Yotsukura, S.I. Watanabe, M. Arai, J. Zenkoh, K. Shiraiishi, M. Seki, A. Kanai, Y. Shiraiishi, Y. Yatabe, D. Matsubara, Y. Suzuki, M. Noguchi, T. Kohno, A. Suzuki, Whole-genome sequencing reveals the molecular implications of the stepwise progression of lung adenocarcinoma, *Nat. Commun.* 14 (2023) 8375.
- [20] F. Wu, X. Zhang, M. Wang, J. Zhang, M. Chen, Z. Ren, M. Wu, P. Song, J. Yu, D. Chen, Deciphering the role of immunoglobulin secreting malignant lineages in the invasive frontiers of small cell lung cancer by scRNA-seq and spatial transcriptomics analysis, *Cell Discov.* 9 (2023) 123.
- [21] Y. Wang, D. Chen, Y. Liu, D. Shi, C. Duan, J. Li, X. Shi, Y. Zhang, Z. Yu, N. Sun, W. Wang, Y. Ma, X. Xu, W. Otkur, X. Liu, T. Xia, H. Qi, H.L. Piao, H.X. Liu, Multidirectional characterization of cellular composition and spatial architecture in human multiple primary lung cancers, *Cell Death Dis.* 14 (2023) 462.
- [22] J. Zhu, Y. Fan, Y. Xiong, W. Wang, J. Chen, Y. Xia, J. Lei, L. Gong, S. Sun, T. Jiang, Delineating the dynamic evolution from preneoplasia to invasive lung adenocarcinoma by integrating single-cell RNA sequencing and spatial transcriptomics, *Exp. Mol. Med* 54 (2020) 2060–2076.
- [23] Y. Kanda, Investigation of the freely available easy-to-use software 'EZR' for medical statistics, *Bone Marrow Transpl.* 48 (2013) 452–458.
- [24] B. Caratti, M. Fidan, G. Caratti, K. Breitenecker, M. Engler, N. Kazemitash, R. Traut, R. Wittig, E. Casanova, M.R. Ahmadian, J.P. Tuckermann, H.P. Moll, I.C. Cirstea, The glucocorticoid receptor associates with RAS complexes to inhibit cell proliferation and tumor growth, *Sci. Signal* 15 (2022) eabm4452.
- [25] M. Dorso, P.T. Patel, A. Pankov, J.A. Boyer, R.K. Soni, I.S. Del Priore, O. Hayatt, A. Kulick, C.J. Hagen, E. de Stanchina, M.R. Junttila, A. Daemen, L.S. Friedman, R. C. Hendrickson, S. Chandrapaty, A druggable FOXA1-glucocorticoid receptor transcriptional axis drives tumor growth in a subset of non-small cell lung cancer, *Cancer Res Commun.* 3 (2023) 1788–1799.
- [26] P. Kay, G. Schlossmacher, L. Matthews, P. Sommer, D. Singh, A. White, D. Ray, Loss of glucocorticoid receptor expression by DNA methylation prevents glucocorticoid induced apoptosis in human small cell lung cancer cells, *PLoS One* 6 (2011) e24839.
- [27] B.C. Freeman, K.R. Yamamoto, Disassembly of transcriptional regulatory complexes by molecular chaperones, *Science* 296 (2002) 2232–2235.
- [28] P. Gao, K. Zou, L. Xiao, H. Zhou, X. Xu, Z. Zeng, W. Zhang, High expression of PTGES3 is an independent predictive poor prognostic biomarker and correlates with immune infiltrates in lung adenocarcinoma, *Int Immunopharmacol.* 110 (2022) 108954.
- [29] W. Jiang, Q. Wei, H. Xie, D. Wu, H. He, X. Lv, Effect of PTGES3 on the prognosis and immune regulation in lung adenocarcinoma, *Anal. Cell Pathol. (Amst.)* (2023) 4522045.
- [30] I. Grad, D. Picard, The glucocorticoid responses are shaped by molecular chaperones, *Mol. Cell Endocrinol.* 275 (2007) 2–12.
- [31] M. Niu, B. Zhang, L. Li, Z. Su, W. Pu, C. Zhao, L. Wei, P. Lian, R. Lu, R. Wang, J. Wazir, Q. Gao, S. Song, H. Wang, Targeting HSP90 inhibits proliferation and induces apoptosis through AKT1/ERK pathway in lung cancer, *Front Pharm.* 12 (2022) 724192.
- [32] L. Wang, H. Zhao, L. Zhang, H. Luo, Q. Chen, X. Zuo, HSP90AA1, ADRB2, TBL1XR1 and HSPB1 are chronic obstructive pulmonary disease-related genes that facilitate squamous cell lung cancer progression, *Oncol. Lett.* 19 (2020) 2115–2122.
- [33] E. Szabo, M.E. Riffe, S.M. Steinberg, M.J. Birrer, R.I. Linnoila, Altered cJUN expression: an early event in human lung carcinogenesis, *Cancer Res* 56 (1996) 305–315.
- [34] J. Yi, B.Z. Pan, L. Xiong, H.Z. Song, Clinical significance of angiotensin-like protein 4 expression in tissue and serum of esophageal squamous cell carcinoma patients, *Med Oncol.* 30 (2013) 680.
- [35] K. Shibata, T. Nakayama, H. Hirakawa, S. Hidaka, T. Nagayasu, Clinicopathological significance of angiotensin-like protein 4 expression in oesophageal squamous cell carcinoma, *J. Clin. Pathol.* 63 (2010) 1054–1058.
- [36] K.H. Chiang, J.M. Shieh, C.J. Shen, T.W. Chang, P.T. Wu, J.Y. Hsu, J.P. Tsai, W. C. Chang, B.K. Chen, Epidermal growth factor-induced COX-2 regulates metastasis of head and neck squamous cell carcinoma through upregulation of angiotensin-like 4, *Cancer Sci.* 111 (2020) 2004–2015.
- [37] C.J. Shen, S.H. Chan, C.T. Lee, W.C. Huang, J.P. Tsai, B.K. Chen, Oleic acid-induced ANGPTL4 enhances head and neck squamous cell carcinoma anoikis resistance and metastasis via up-regulation of fibronectin, *Cancer Lett.* 386 (2017) 110–122.
- [38] Y.H. Liao, K.H. Chiang, J.M. Shieh, C.R. Huang, C.J. Shen, W.C. Huang, B.K. Chen, Epidermal growth factor-induced ANGPTL4 enhances anoikis resistance and tumour metastasis in head and neck squamous cell carcinoma, *Oncogene* 36 (2017) 2228–2242.
- [39] J. Tanaka, T. Irié, G. Yamamoto, R. Yasuhara, T. Isobe, C. Hokazono, T. Tachikawa, Y. Kohno, K. Mishima, ANGPTL4 regulates the metastatic potential of oral squamous cell carcinoma, *J. Oral. Pathol. Med* 44 (2015) 126–133.
- [40] Z. Huang, J. Xie, S. Lin, S. Li, Z. Huang, Y. Wang, J. Ye, The downregulation of ANGPTL4 inhibits the migration and proliferation of tongue squamous cell carcinoma, *Arch. Oral. Biol.* 71 (2016) 144–149.